Lee region of Gran Canaria

Eric D. Barton,[1] Gotzon Basterretxea,[2] Pierre Flament,[3,4] E. Gay Mitchelson-Jacob,[5] Bethan Jones,[5] Javier Arístegui,[2] and Felix Herrera[6]

Abstract. The mountainous Canary Islands present obstacles to the trade winds and to the Canary Current flowing equatorward past them. In situ observations of hydrographic properties and surface winds south of Gran Canaria, together with advanced very high resolution radiometer and synthetic aperture radar images during 2 weeks in summer 1995 are analyzed. A cyclonic eddy shed from the west of the island drifted southwestward at 5 cm s^{-1}, while the southeast coast was approached by an upwelling filament originating off NW Africa. A wind lee region bounded by intense horizontal shear lines had a weak return islandward wind in its center. The lee formed a triangular, diurnally varying, warm water pool with two sea surface temperature maxima separated by lower temperatures below the return wind. Shallow temperature stratification occurred behind the island in contrast to the uniform surface mixed layer in exposed regions. Upwelling and downwelling of 10 - 20 m d^{-1} were indicated on the cyclonic and anticyclonic sides of the lee region. In the SAR images, lines of strong current shear along a temperature front between the cyclonic eddy and the upwelling filament were identifiable. However, the radar images were dominated by atmospheric phenomena, including mountain lee wave packets, windrows, and wind shear lines. Estimation of the wind field from the SAR backscatter intensity revealed complex structure and intensification on the edges of the warm lee.

1. Introduction

The Canary Island archipelago, which rises steeply from ocean depths of over 3000 m, forms an obstacle to the southwestward flows of both the Canary Current and the trade winds (Figure 1). The summit of Tenerife is at 3717 m, while that of Gran Canaria reaches 1949 m. The presence of lee regions behind the islands has long been recognized; becalming downwind of Gomera, Tenerife and Gran Canaria in August-September 1492 delayed Columbus' departure on the *Santa María* to discover the New World [*Columbus*, 1987].

The meteorology of the Canary Islands has been summarized by *Naya* [1984]. From March to September the trade winds are capped by an atmospheric temperature inversion between 400 and 1000 m. As the approaching air stream is forced up the slopes of the islands, a layer of stratocumulus is often formed at the base of the inversion. The stable inversion layer prevents the air from rising farther and diverts the flow around the island flanks. Some of the diverted flow is channeled back to the coasts down deep canyons to converge with the main flow, increasing wind speed and causing vertical motion and cloud production. Even at times of extensive

stratocumulus the leeward coasts often remain clear because of subsidence down the lee slopes.

Warm oceanic "wakes" have been identified in satellite images as anomalously high surface temperature regions in the island lees [*Hernández-Guerra*, 1990; *Van Camp et al.*, 1991]. The extent of the wakes, which varied from island to island, was attributed to the differing heights of the islands. Wake orientation followed the prevailing winds. Wakes formed during the day by solar heating and weakened or disappeared in night time images. They were bounded by temperature fronts, presumably coincident with the boundary between the trade winds and the calm.

In this paper we report in situ observations of hydrographic structure and surface winds downstream of Gran Canaria and remote sensing advanced very high resolution radiometer (AVHRR) and synthetic aperture radar (SAR) imagery during 2 weeks of the strongest summer trade winds. Repeated sampling revealed the strong wind shear lines, the associated thermohaline structure, and the subsurface pycnocline distortion caused by Ekman pumping. The variability of the wake in relation to the larger-scale context and to features in the AVHRR and SAR images is discussed. Both atmospheric and oceanic phenomena have signatures in the radar images. The wind field inferred from the SAR backscatter intensity shows strong structure related to the extent of the warm lee.

2. Methods

Between July 24 and August 8 1995, conductivity-temperature-depth (CTD) sections spanning the lee region of Gran Canaria were made on eight occasions (Figure 1). Each consisted of 5 - 9 profiles to 200 m depth spaced at 4 km intervals from the lee into the open ocean trade winds. Six sections were made on the western (cyclonic) half, and two were made on the eastern (anticyclonic) half. The recently calibrated Seabird SBE 19 CTD and Sea Tech fluorometer

[1] School of Ocean Sciences, University of Wales, Bangor, UK.
[2] Facultad de Ciencias del Mar, Universidad de Las Palmas de Gran Canaria, Las Palmas de Gran Canaria, Spain.
[3] Department of Oceanography, University of Hawaii at Manoa, Honolulu.
[4] Also at Département d'Océanographie Spatiale,IFREMER, Brest,France
[5] Unit for Coastal and Estuarine Studies, University of Wales, Bangor, UK.
[6] Laboratorio de Comunicaciones y Teledetección, Universidad de La Laguna, Tenerife, Spain
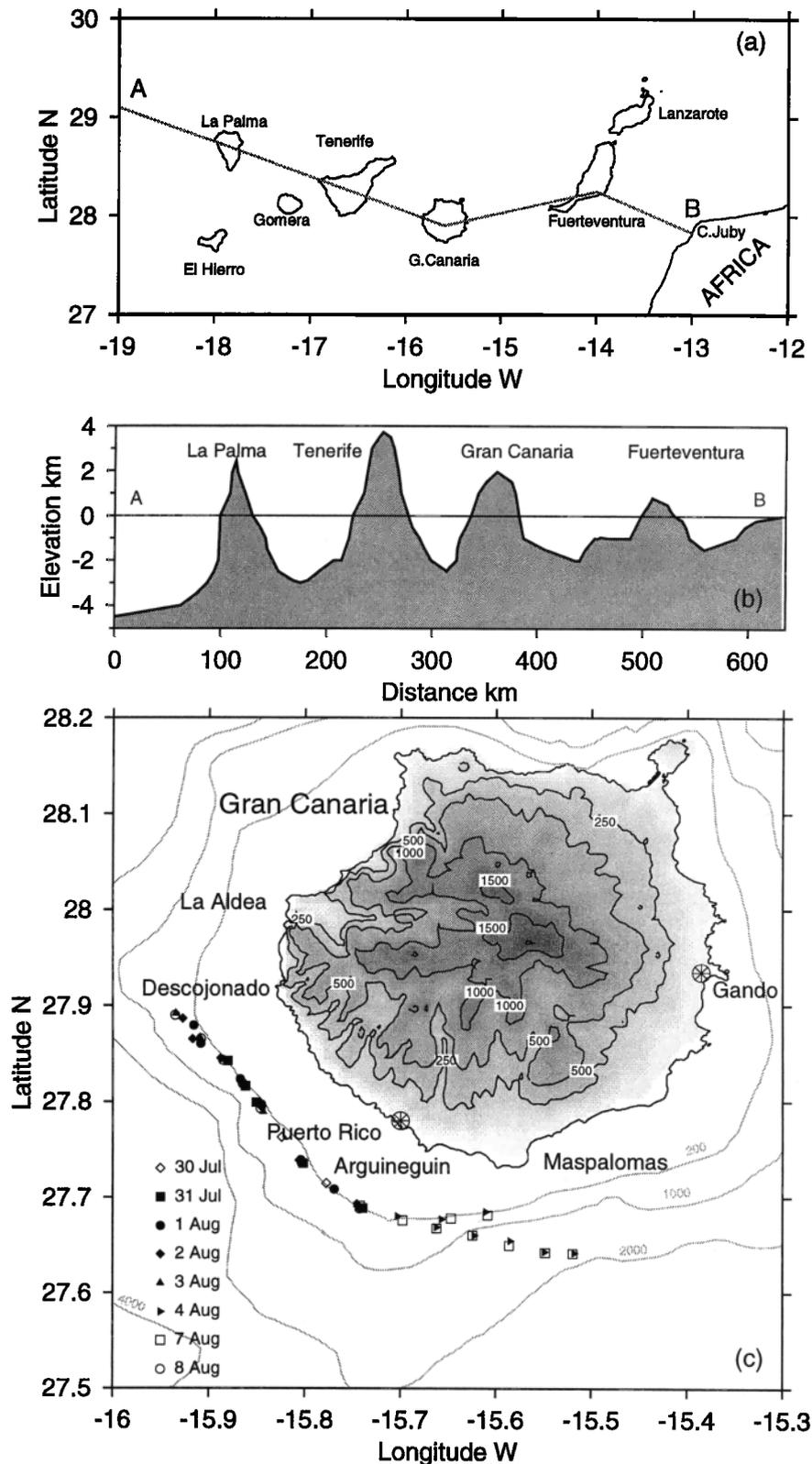
Figure 1. (a) The Canary Island archipelago lies < 100 km off the African coast. (b) Elevation profile along the line AB in Figure 1a. (c) Conductivity-temperature-depth station positions. The island and sea bed topography is shown in meters. Time series of wind were recorded at island sites marked by asterisks.

performed within specifications. The small research vessel could work only by day and only a few kilometers into the full strength of the trades.

On the vessel, relative wind velocity, air temperature, and atmospheric pressure were recorded at 1 min intervals ~ 10 m

above sea level. The average speed, temperature, and pressure and the most frequent wind direction were recorded in each interval. The ship's latitude and longitude from a Magellan 1200 Global Positioning System navigator were logged every 2 s. The positions were edited following *Fleming and Hill*
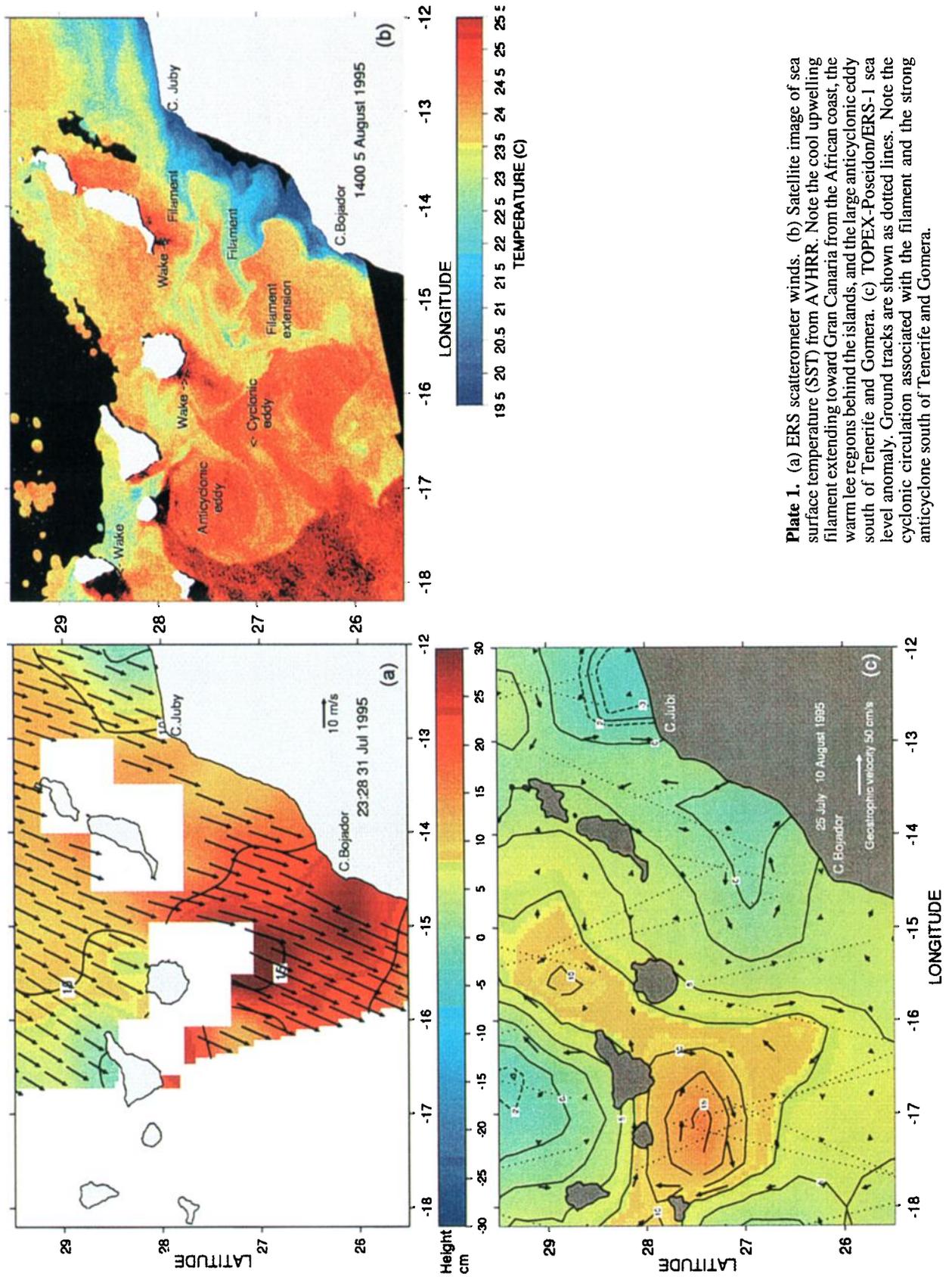
Plate 1. (a) ERS scatterometer winds. (b) Satellite image of sea surface temperature (SST) from AVHRR. Note the cool upwelling filament extending toward Gran Canaria from the African coast, the warm lee regions behind the islands, and the large anticyclonic eddy south of Tenerife and Gomera. (c) TOPEX-Poseidon/ERS-1 sea level anomaly. Ground tracks are shown as dotted lines. Note the cyclonic circulation associated with the filament and the strong anticyclone south of Tenerife and Gomera.

[1982] to remove spurious values, reduce the noise level, and provide smoothed estimates every minute. The ship's velocity obtained by differencing subsequent positions yielded absolute wind velocity.

Wind velocities reported four times per day at 10 sites around the island were obtained for July and August. The Aeropuerto de Gran Canaria site at Gando on the low-lying east coast (Figure 1) is well exposed to the summer trade winds (Figure 2a), so is representative of the surrounding open ocean region. The airport wind record (Figure 2b) also indicates the timing of the CTD observations and the satellite images. The record from Puerto Rico (Figure 2c) represents conditions in the center of the lee coast, completely sheltered from the strong trades.

AVHRR images were captured four times daily at the Universidad de La Laguna high resolution picture transmission receiving station in Tenerife. The raw data were subsequently geolocated using the satellite orbit elements and adjusted using the island coastlines to reach a final ground location accuracy of ~ 2 km. Sea surface temperatures were then estimated from the five-channel records using the algorithm of McClain et al. [1985] to correct for atmospheric water vapor to an absolute precision better than 1°C. Clouds were detected and flagged using a combination of tests, including a textural test on the visible and infrared channels to detect small cumulus clouds and a differential test on the infrared channels to detect fog and low stratus clouds [Saunders and Kriebel, 1988]. The final cloud-masked SST images were remapped to a common Mercator grid, to eliminate geometric distortions due to earth rotation and curvature. The performance of the SST algorithm was checked over an area ~ 100 km x 200 km southwest of Tenerife, which remained cloud-free during the entire period, presumably as a result of air subsidence in the lee of the tallest island. The median temperatures computed for each image over this area indicated a bias of -0.35°C for NOAA 12 and - 3°C for NOAA 9, using NOAA 14 as reference. The NOAA 12 and NOAA 9 images used here were corrected for these biases. The standard deviation of the corrected series of medians was 0.8°C.

SAR scenes were available for July 29 and 30 from ERS-1 and ERS-2, respectively. SAR intensities were converted to normalized radar backscatter cross section (NRSC) following procedures similar to Lehner et al.'s [1998]. The procedures differ slightly for the two satellites but involve correction for saturation in the analog to digital convertor of the satellite receiver in areas of relatively high backscatter [Meadows and Wright, 1994]. Correction is necessary because the prevalent wind speeds (>10 m s⁻¹) are high enough here to provoke saturation. Before application of the recalibration, intensities were smoothed to reduce "speckle" with an 8 x 8 convolution filter and then subsampled at every eighth pixel, increasing image pixel size to ~ (100 m)2. The smoothed intensities were calibrated using the method of Laur et al. [1997] to produce images of calibrated backscatter (in dB). From these, fields of estimated wind speed were determined by application of the empirical C band CMOD4 model developed originally for the ERS scatterometer by Stoffelen and Anderson [1997]. As discussed later, an assumed wind direction is a necessary input to the model as the SAR illuminates the targets in only one narrow range of directions as opposed to three widely separated ones for the ERS scatterometer.

3. Results

The synoptic situation on July 30 (Figure 2a) illustrates the Azores High and Saharan Low typical of boreal summer. The

northeast-southwest trending isobars of the trade wind regime dominated the observation period. Winds at the Aeropuerto de Gran Canaria (Figure 2b) had a vector mean speed of 10.1 m s⁻¹ during the months of July and August. The vector mean direction was 203°, coincident with the principal axis of variance of the wind fluctuations. A weak sea breeze regime had zonal and meridional amplitudes 2.1 and 1.6 m s⁻¹, respectively. The standard deviation of speed was ~ 3 m s⁻¹. Speed increased slightly to a maximum of 16.9 m s⁻¹ on July 30, then decreased similarly through August.

Near Puerto Rico, on the southern lee coast, the July-August winds were weak and, on average, onshore (Figure 2c). The sea breeze regime there had zonal and meridional components of 0.5 and 1.7 m s⁻¹, respectively. The mean vector wind was 0.7 m s⁻¹ toward 28°, with standard deviations in both eastward and northward components exceeding 2 m s⁻¹. The orientation of the principal axis was 315°. No trend in wind speed was evident.

3.1 Regional Context

The relative uniformity and strength of winds over the open ocean during the observation period are shown in Plate 1a, where ERS scatterometer winds are plotted for July 31. The overall direction was southwest, and wind speeds were stronger than 10 m s⁻¹ in much of the area, exceeding 15 m s⁻¹ southeast of Gran Canaria. The low spatial resolution and crude land masking does not permit examination of near-island effects. The overall current in the region is the slow southwestward drift of the Canary Current, but energetic mesoscale structure is indicated by the SST patterns and sea level anomalies (Plates 1b and 1c).

The sea level anomaly (SLA) field, from the combined TOPEX-Poseidon/ERS-1 observations [Le Traon et al., 1995], was derived for the period July 25 to August 10 1995. Only the data from the ERS-1 half cycle corresponding most closely in time to the TOPEX-Poseidon data were used. This was to reduce the smearing of features owing to temporal changes over the 35 day cycle period, albeit at the cost of higher spatial resolution. Ground tracks, shown in Plate 1c as dotted lines, are irregularly distributed and data near land are rejected because of the possibility of signal saturation. The data were smoothed and interpolated to a regular grid using the Barnes algorithm [Koch et al., 1983] before contouring and calculating the geostrophic velocity vectors. The original data are noisy, but the major features of the anomaly field correspond well to those of the SST image.

The SST image of early afternoon August 5 (Plate 1b) show a complex upwelling filament extending out from the African coast, several eddy-like structures, and warmer regions extending southwestward from most of the islands. The filament, arising from the coastal upwelling between Cape Bojador and Cape Juby, has been observed in different years [Barton et al., 1998]. The cyclonic circulation associated with the filament and its extension southward and shoreward is evident in the SLA map (Plate 1c). A second filament apparent near latitude 26°N also coincides with offshore motion. Such filaments frequently carry cooler upwelled waters far offshore. In this case the Juby filament has two cool cores that almost reach Gran Canaria. There they turn southward and merge to approach the African coast again. Such double structure has been observed in Coastal Zone Color Scanner images by Hernández-Guerra et al. [1993]. The flow associated with a similar filament in August 1993 was >50 cm s⁻¹ in the near-surface cold core [Navarro Pérez, 1996], somewhat faster than is indicated in the SLA map.
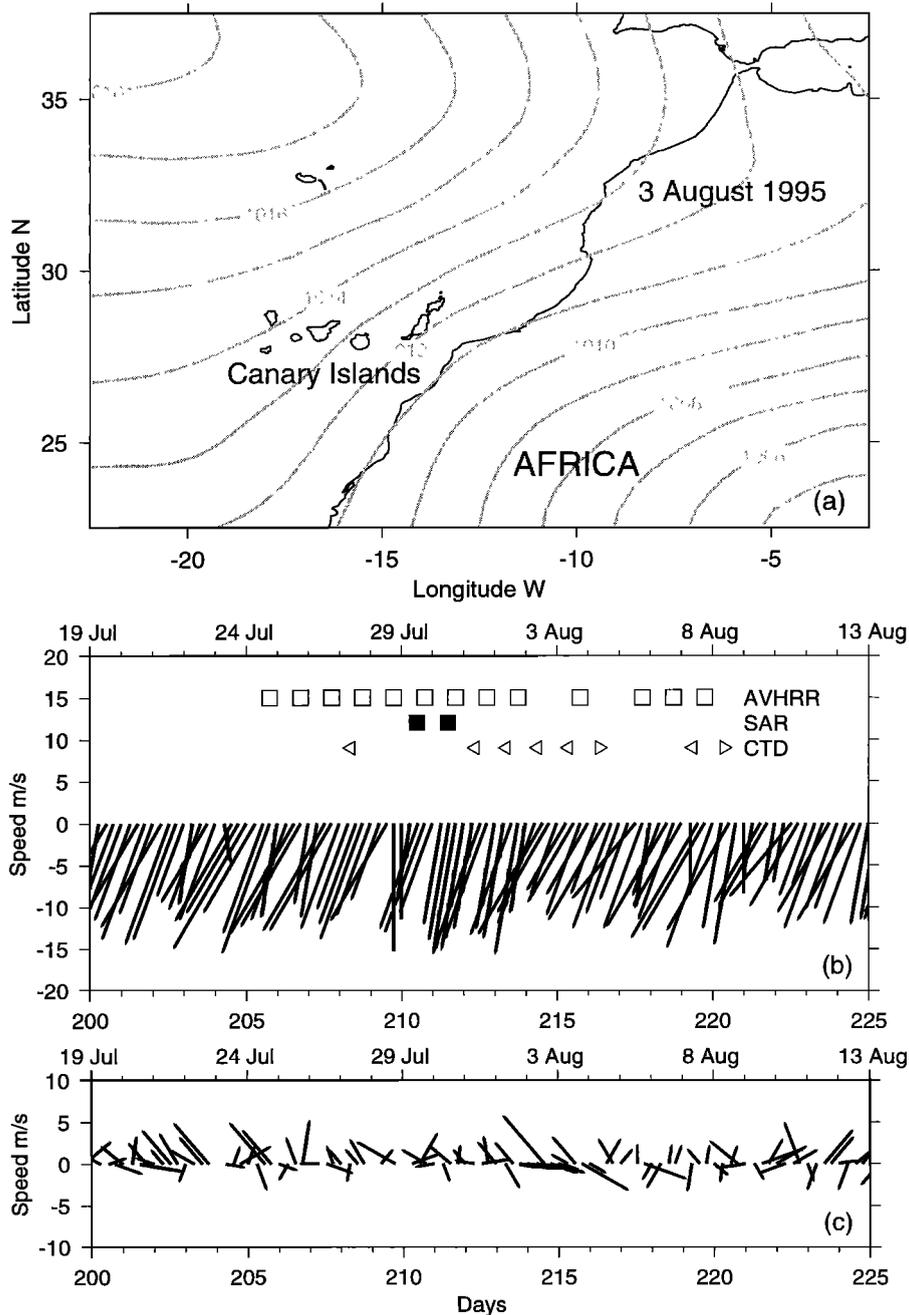
Figure 2. (a) Surface pressure map for July 30 1995. The strong gradient between the Azores High and Saharan Low is related to the trade wind regime. (b) Wind velocity time series from the airport at Gando on the east coast of Gran Canaria. Year day and date labels refer to the larger ticks. The positive y-direction indicates north. Days when advanced very high resolution radiometer (AVHRR) imagery was obtained are marked by open squares, days of synthetic aperture radar (SAR) images are marked by solid squares, and CTD samplings are marked by open triangles pointing left and right for western and eastern surveys, respectively. (c) Wind velocity time series from Puerto Rico on the south coast.

The eddy and warm lee features represent flow disturbance caused by the islands. The 100 km diameter anticyclone south of Tenerife (Plate 1b) has entrained streamers of warmer water from the lee of Gomera and cooler water from the channel south of Tenerife around its northern periphery. Cooler water is entrained generally around its southern edge. In the SLA map (Plate 1c), azimuthal geostrophic velocities up to 0.4 m s^{-1} occur around the anticyclone. The centripetal acceleration was not taken into account and could result in a supergeostrophic

increase of ~ 20% given the radius of the feature. The good definition of this feature is partly caused by its persistence and fixed location. Similar anticyclones were observed in 1993 when a drifter traced its periphery with velocities close to 1 m s^{-1} [*Barton et al.*, 1998] and in 1996 by *Molina et al.* [1998].

Southeast of the anticyclone are traces of a cold-core cyclonic eddy shed from Gran Canaria. Younger, smaller cyclones are located west of Tenerife and La Palma. Similar structures, and their effect on primary production, are de-

scribed by *Aristegui et al.* [1997]. These cyclones and other details of the flow patterns suggested by the SST field, like the small instabilities on the southern boundary of the filament, are generally not apparent in the SLA field because they are small relative to the gap between ground tracks. Though the altimetry map is of anomalies with respect to a 3 year mean topography, the weak mean flow [*Navarro-Pérez and Barton*, 1998] allows detection of larger mesoscale structures seen in the SST map.

West coast waters off each island are cooler than east coast waters because of upwelling and downwelling caused by the trade wind-driven westward Ekman transport. Upwelling off western Fuerteventura was observed in situ by *Molina and Laatzen* [1989]. Behind Gran Canaria and other islands an almost triangular region of warmer surface water extends up to 100 km in the direction of the winds. The warm features result from the absence of wind mixing and the consequent production of a diurnal near-surface thermocline and associated elevated surface temperatures [*Flament et al.*, 1994]. Late night and early morning images do not show the feature as strongly, although it does not disappear completely.

3.2 Wind Structure in the Lee

The in situ winds across the lee of Gran Canaria (Figure 3) have been rotated into the principle axes of variance of the ship wind data set. A vector drawn vertically down the page is therefore directed toward 225°. The 20° difference between principal axes of the airport and ship winds reflects spatial variability of wind in the lee. An ill-defined reverse flow in the center of the lee on July 31 and August 7 suggests
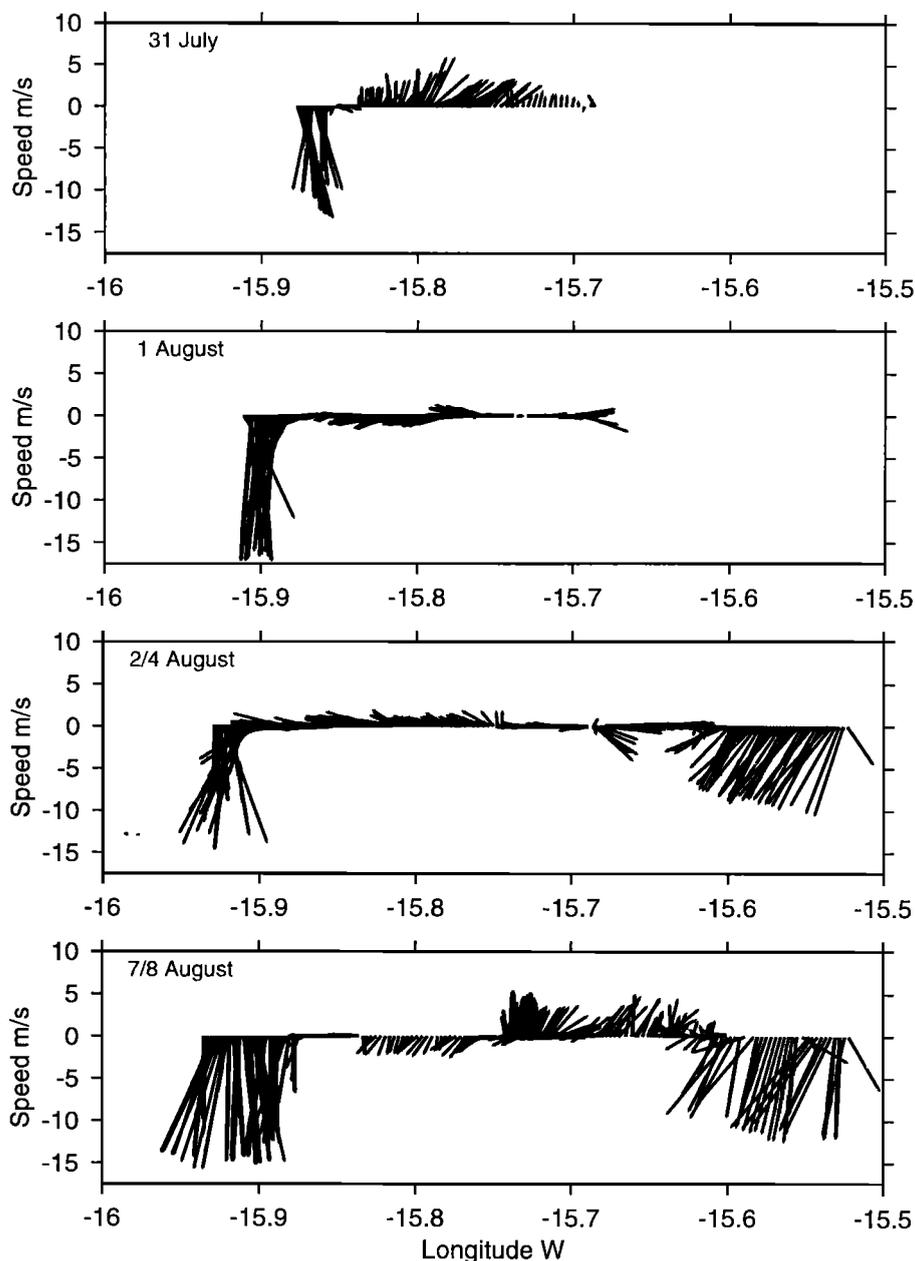
Figure 3. Profile of 10 m ship winds across the lee of Gran Canaria in August 1995. Strong shear zones bound the zone of weak recirculation in the lee. Flow is convergent towards both boundaries.

counterrotating eddies behind the island. In the strong shear zones on the lee boundaries, speed increases from 0 to 15 m s⁻¹ in distances of ~2 km.

In most transects the cross-stream component of surface wind was convergent toward the shear boundary on both sides of the lee. The consequent upward motion of humid surface air characteristically forms narrow bands of cloud at the base of the inversion layer along the edges of the lee. Given the measured 10 m height values of relative humidity ~ 60%, atmospheric pressure around 1016 mbar, and air temperature of ~ 23°C, saturation would be reached at ~ 900 m, typical of the low level cloud strip. Midday radiosonde reports from Tenerife indicated inversion layer base heights between 850 and 1000 m. Such low-lying cloud features are seen in several satellite images, but they are often undetected because their width is less than the AVHRR resolution. In most transects the surface pressure dropped by 1 to 2 mbar on crossing the shear zone into the exposed region, consistent with convergence at the boundary.

3.3 Near-Surface Temperature Profiles

Sea surface CTD temperatures (Figure 4a) reveal the warm surface lee region and its strong boundaries. Contrast between the sheltered and exposed surface waters is slightly less than 1.5°C, although surface temperature in the lee is underestimated because the first CTD record was usually at several meters depth. Scatter in the distribution reflects differences in time of sampling and shifts in boundary position. A few stations were sampled in the early morning before insolation had time to warm the surface after night time heat loss and convective overturning. The position of the wind shear lines coincides with the strongest horizontal temperature gradients.

Temperature profiles (Figure 4b) from August 2 show subsurface differences between the trade wind and lee regions. In the exposed region, at the westernmost position, station 401, a well-mixed surface layer was bounded at 25 m depth by a strong thermocline. Just inside the wind boundary, station 403, a warmer, weakly stratified near-surface zone had developed above the mixed layer in response to diurnal heating and weaker wind. At 20-30 m depth, temperatures were similar to the previous station but the thermocline was twice as deep, at 65 m. In the center of the lee, station 405, the surface layer was considerably thicker with temperatures at all depths higher than elsewhere as a result of accumulated warming. The main thermocline was depressed to ~ 125 m, and there was evidence of nocturnal shallow overturning down to 20 m moderated by subsequent daytime surface warming. A similar progression was evident on the eastern anticyclonic boundary.

The pycnocline, estimated from the first maximum in Brunt-Vaisala frequency below the diurnal pycnocline (Figure 4c), showed a strong depression in the center of the island lee and shoaling to its sides, particularly to the west. Its depth ranged between 25 and 135 m over a distance of 15 km. Mean pycnocline depth in the undisturbed far field away from the islands is around 70 m in summer [Arístegui et al., 1997], so anomalies associated with the lee were 50 - 60 m. Pycnocline depth was consistent throughout the sampling period except for an eastward shift of the structure in the last composite section August 7-8. Lentz [1992] observed that the surface mixed layer depth h in the NW African and other coastal upwelling regions was predicted remarkably well by the one-dimensional parameterization of Pollard et al. [1973]:

$$h = A\, u_* /(N f)^{1/2},$$

where the shear velocity $u_* = (\tau/\rho)^{1/2}$, τ is the wind stress, ρ is water density, N is the Brunt Vaisala frequency at the base of the mixed layer, f is the Coriolis parameter and A is a constant.

Taking observed values, in our case this formulation indicates a deeper mixed layer around 20 m in the exposed zones and a shallower layer about 5 m thick in the lee (Figure 4c). The predicted mixed layer depth was roughly as observed on the western end of the section, i.e., ~ 5 m less than the pycnocline depth, but was much shallower than pycnocline depth in the lee and at the eastern end. This is to be expected since the pycnocline is being upwelled in the west, where conditions similar to those of Lentz apply, and depressed in the east, where the surface mixed layer is independent of the main pycnocline.

3.4 Water Column Response

Sections for August 3-4 and August 7-8 (Figures 5 and 6, respectively) show the strong deepening of the thermocline and pycnocline behind the island in the center of the warm region. The earlier sections (not shown) across the western half of the lee region presented similar characteristics. Figure 5 shows the pycnocline to deepen from 40 m at the ends of the line to 95 m in the center. In the section of August 7-8 (Figure 6) the pycnocline shows a similar deepening in the western half of the section but remains near 80 m in the eastern half. The warm (>22.5°C), less dense (<25.3 kg m⁻³) surface waters of the lee were clearly seen in all the sections.

In the earlier section (Figure 5) higher salinity was found to the east in the layers above 120 m but 3 days later was found to the west (Figure 6); this is especially clear in the salinity versus density plots. Over all the sections, salinity in the upper pycnocline near the 25.5 kg m⁻³ isopycnal ranged by 0.3 practical salinity units, indicating a variety of sources for water in the lee. Geostrophic velocities relative to the deepest available data at 200 dbar indicated a northward flow component in the western half of both sections and a southward one in the eastern half. The latter introduces low-salinity water from the upwelling filament, while the northward flow could bring in saline oceanic water.

A weak deep chlorophyll maximum (DCM) showed maximum values over 0.6 mg m⁻³ at the westernmost stations in the earlier sections. Chlorophyll at the sea surface was generally < 0.1 mg m⁻³ in the lee of the island and only marginally higher in the well-mixed exposed stations. The depths of the DCM and the pycnocline were not significantly correlated. The DCM in the lee of the island occurred above the pycnocline (density anomaly ~ 25.7 - 26.0 kg m⁻³), whereas in the exposed regions it occurred below. This is possibly a phytoplankton response to the lower light levels associated with depression of the interface but more likely reflects different phytoplankton communities with different light and nutrient histories. The eastward shift of the deeper wake structure between August 3-4 and 7-8 is again evident.

3.5 Sea Surface Temperature Imagery Sequence

Corrected SSTs from early afternoon passes of the NOAA 14 satellite show the variation of cyclonic eddy, warm lee, and cool filament between July 24 and August 7 (Plate 2). Because the NOAA 14 pass of August 7 was cloud-contaminated, the evening pass of NOAA 9 is included. Midday
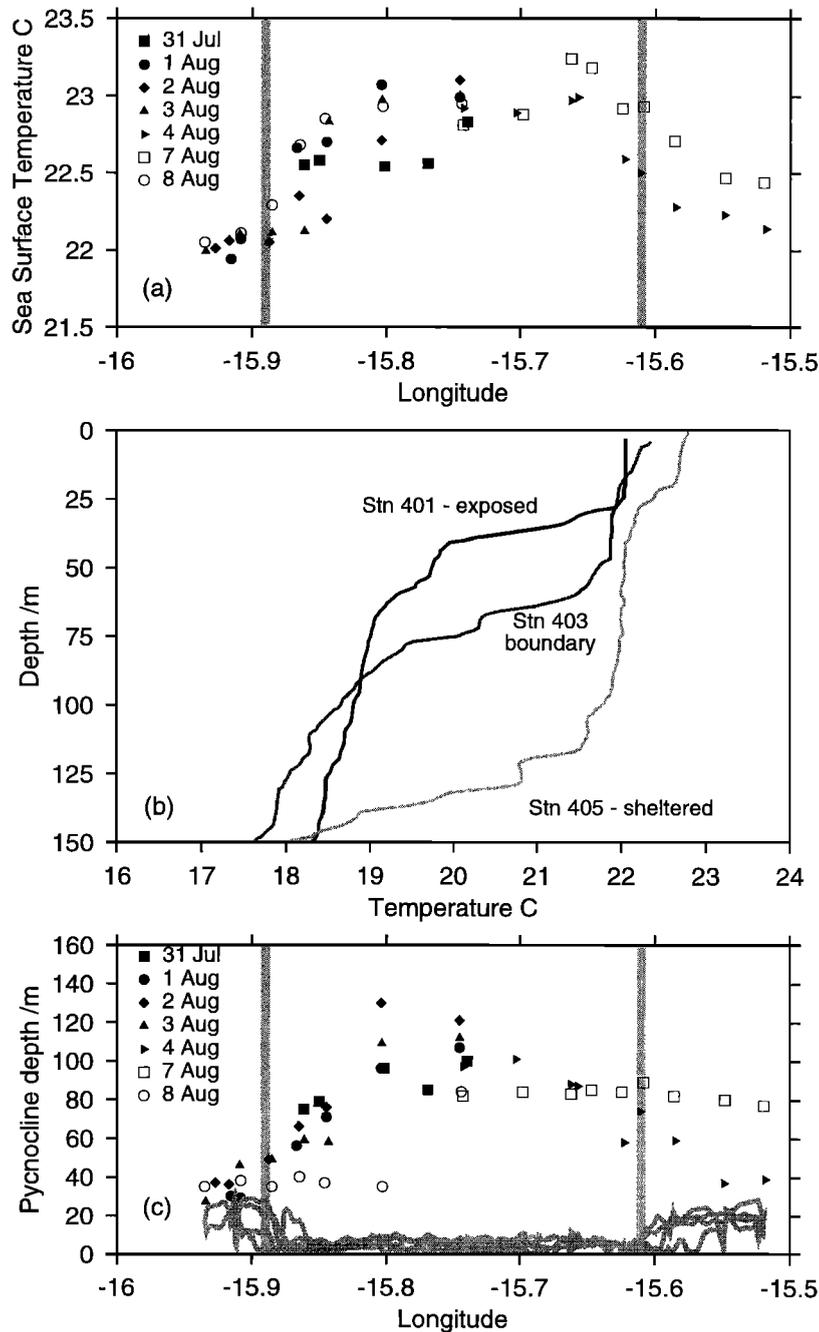
Figure 4. (a) Variation of CTD surface temperature across the lee region. The approximate position of the wind shear zone is indicated by wide vertical lines. (b) Vertical profiles of daytime temperature from the sheltered (station 405), boundary (station 403) and exposed (station 401) regions showing near-surface warming and thermocline depression in the lee. (c) Variation of pycnocline depth across the lee region. The position of the wind shear zone is indicated as in Figure 4a. The grey curves show mixed layer depth estimated from wind stress.

winds at island sites and subsampled ship winds (taken between 0800 and 1300 UT) are shown when available.

Winds at two sites in the northeast and northwest fluctuated widely in direction because of upwind topography, but most sites showed consistent speed and direction patterns. The strongest winds occurred around the end of July, when SSTs decreased noticeably. Temperatures were warmer on August 3 and 5 when winds weakened slightly. Cloud cover often obscured the northern coasts of the island, but the south coast remained cloud-free. The generally well defined warm lee was

closely aligned with the predominant wind direction. Its length and overall shape were variable.

Close to the lee coast, an area of higher temperature occurred southwest of Arguineguin and a more persistent one occurred south of Punta Descojonado. On July 31, the western patch coincided with a region of null or weak shoreward winds. Slightly cooler temperatures in the center of the lee coincided with strongest shoreward winds. The eastern boundary of the lee was generally marked by a line of strong temperature contrast paralleling the east coast winds. All the
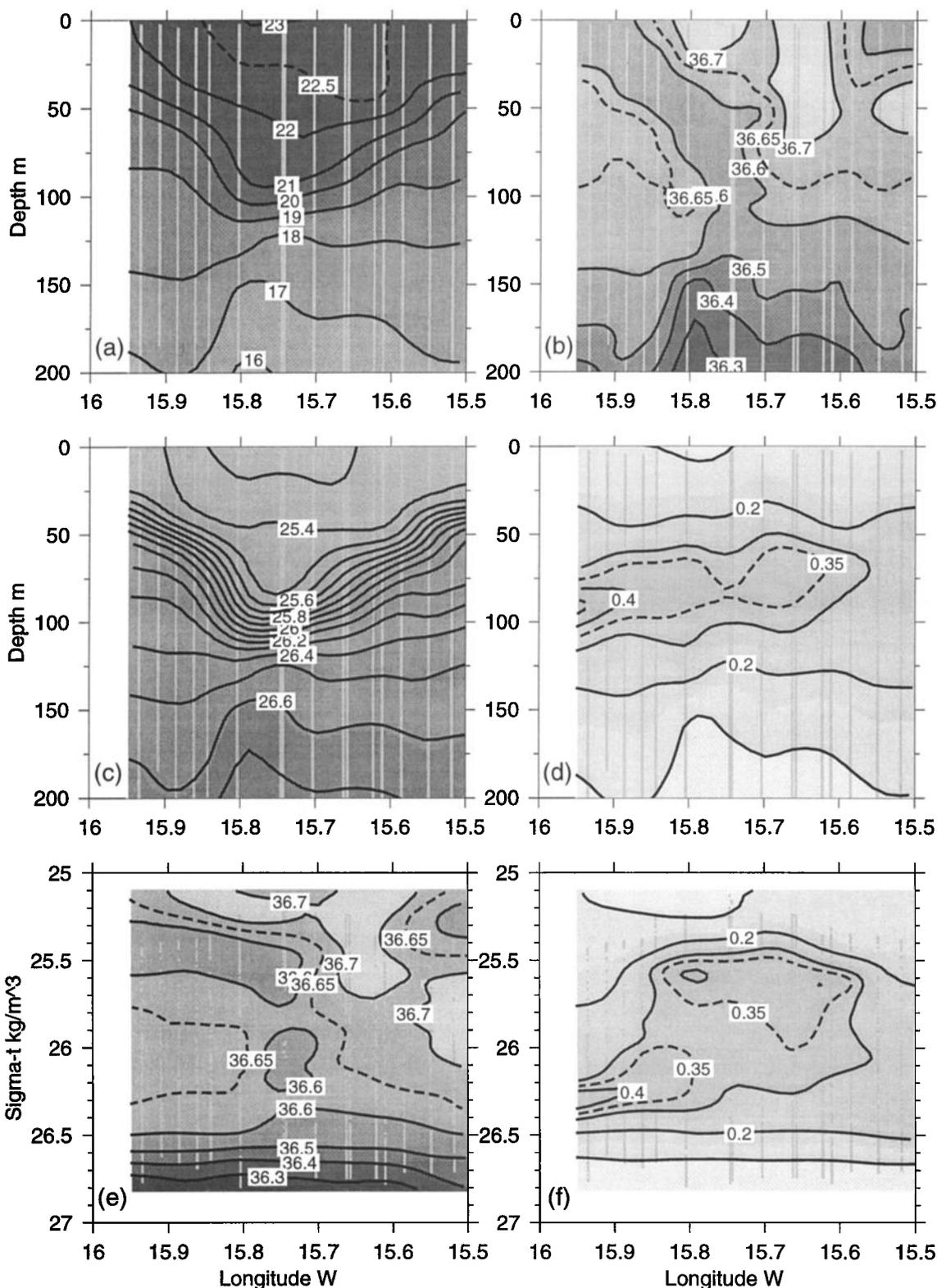
Figure 5. Depth sections of (a) temperature, (b) salinity, (c) density, and (d) chlorophyll and corresponding isopycnal sections of (e) salinity and (f) chlorophyll across the lee region made on August 3-4 .

images show surface waters cooler off the west of Gran Canaria than off the east, because surface Ekman transport provokes upwelling and downwelling, respectively.

The cyclonic eddy became less distinct as it moved southwestward at ~ 0.05 m s⁻¹. By August 7, when it reached the southern edge of the area shown, its surface temperature signal was virtually indistinguishable. Initially, the eddy and filament were separated by a narrow band of warmer waters from the lee and farther south, entrained around the north and east of the eddy. This band widened as the eddy moved away.
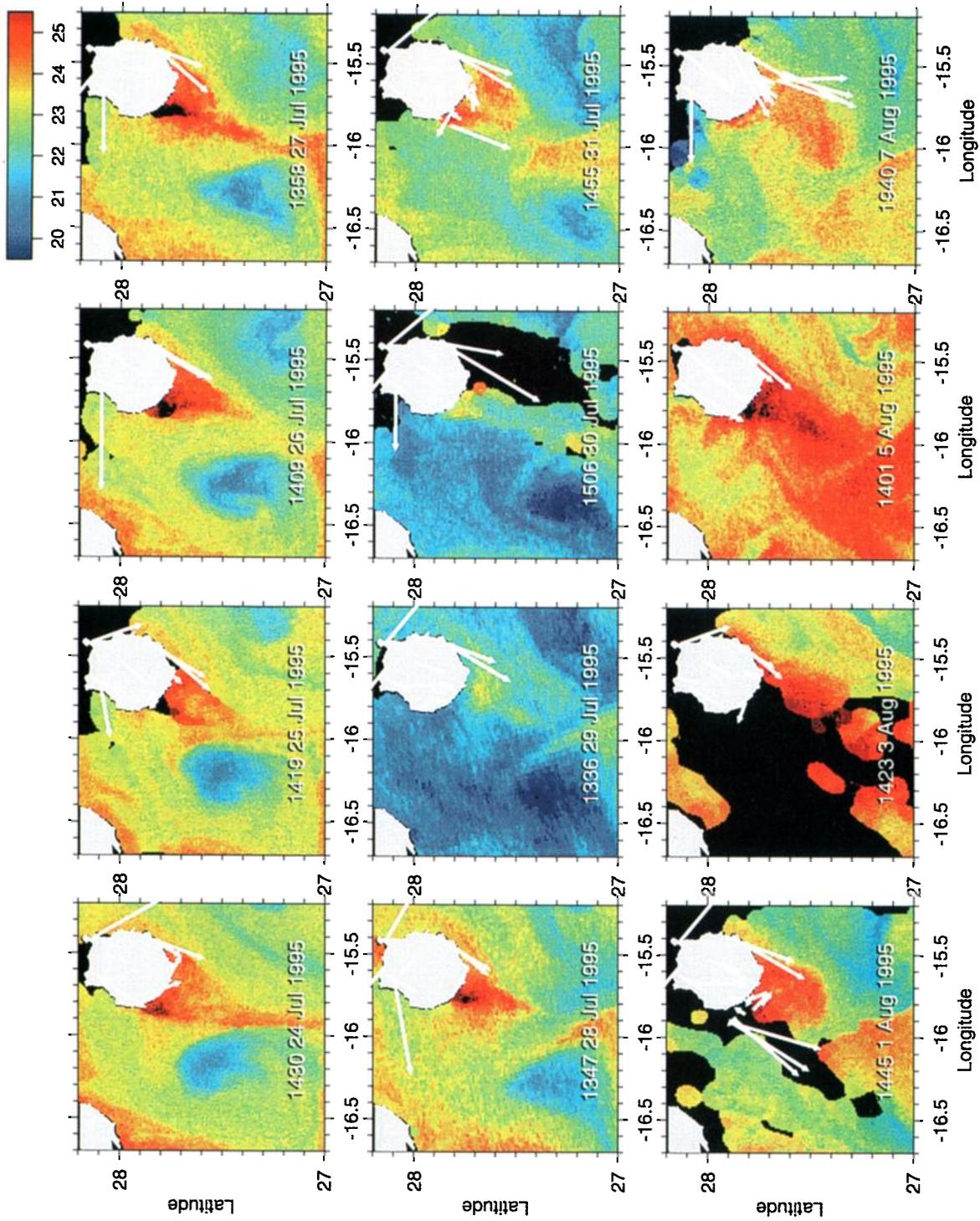
Plate 2. Early afternoon AVHRR SST images showing development of the downstream area of Gran Canaria from July 24 to August 7 1995. Midday shore and ship winds are shown where available.
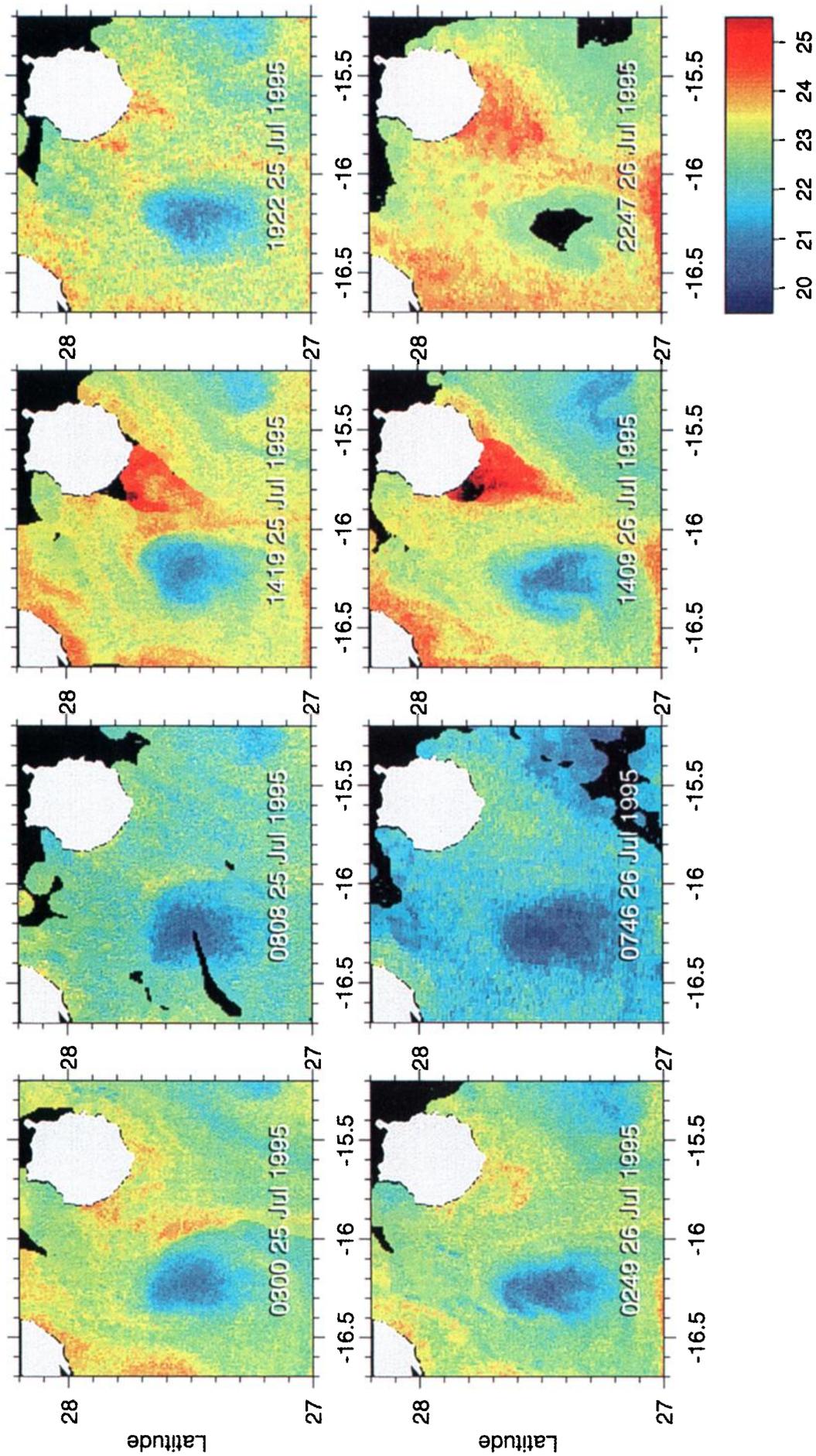
Plate 3. AVHRR SST images for July 25 and 26 1995, showing diurnal development of the warm lee of Gran Canaria.

Throughout the period, two cores of cooler filament waters entered from the northwest and merged as they turned south. The southern core of cooler water was persistently stronger. Both showed variation in small-scale structure.

A sequence of images for July 25 and 26 shows the diurnal development of the surface temperature signature of the lee (Plate 3). The coolest temperatures were observed in the image just after sunrise (~0808 UT) when virtually no wake
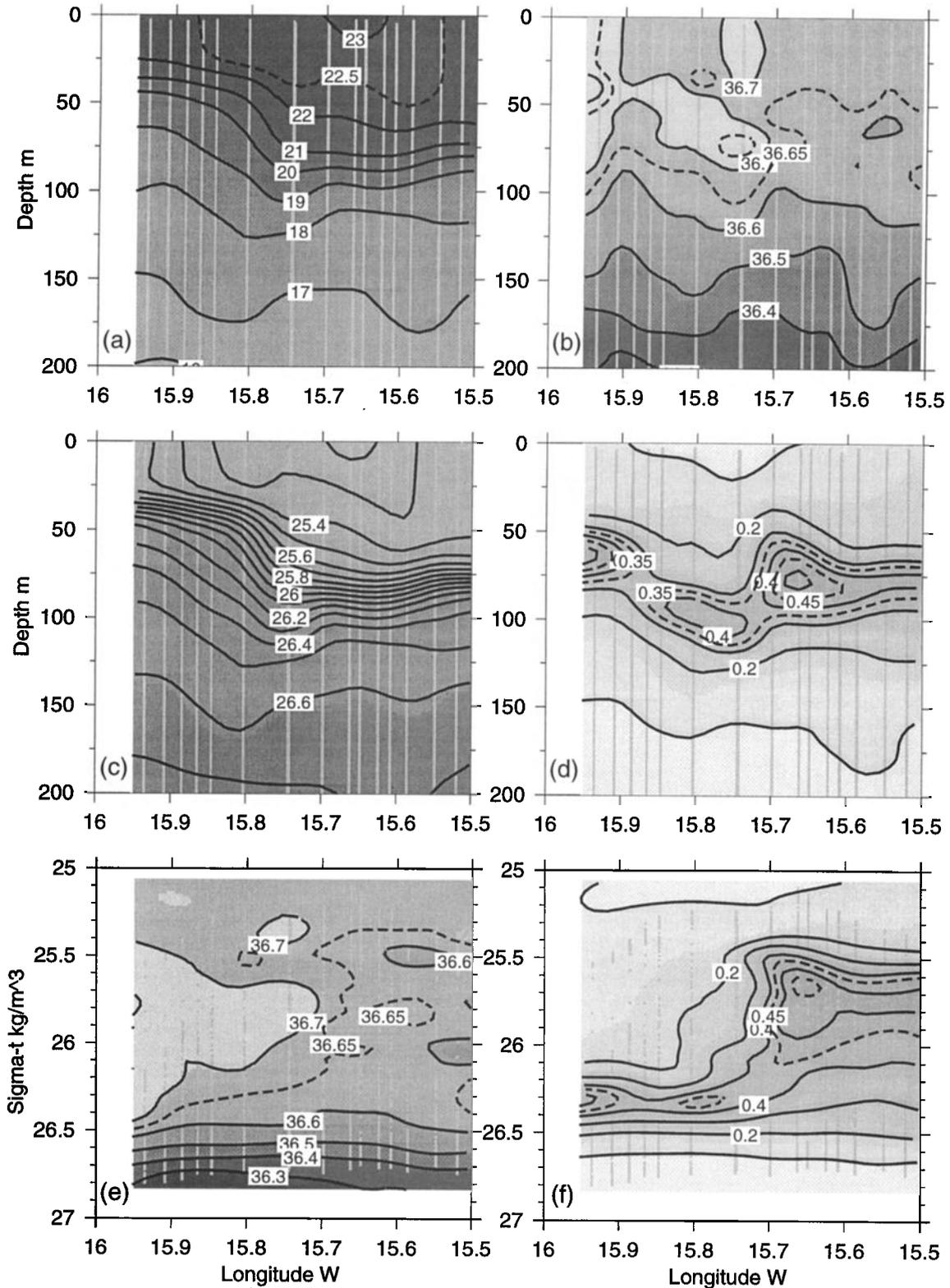
Figure 6. Depth sections of (a) temperature, (b) salinity, (c) density, and (d) chlorophyll and corresponding isopycnal sections of (e) salinity and (f) chlorophyll across the lee region made on August 7-8.

anomaly was visible. By early afternoon (~1400 UT) a clearly defined wake region was established with sharp lateral boundaries. These had weakened by midevening (~2000 UT) to a diffuse anomaly that weakened gradually through the night, persisting until at least ~0300 UT on both days.

3.6 SAR and SST Features

The first pair of images (Figure 7a and 7b) depicts the SST on July 29 at 1050 UT and surface roughness 50 min later. Midday shore winds, superimposed, show the strong trades at east coast sites, weaker winds at inland elevations, and a reverse or zero flow on the lee coast. SSTs ranged between 19.5 and just over 22°C. The slightly warmer island wake extended some 60 km southwestward from Arguineguin as a narrow "tail" (TT' in Figure 7a) to intersect the tongue of warmer oceanic water entrained around the cold core eddy centered near 27.3°N, 16.3"W. Southeast of Gran Canaria, the offshore limit of the double-core upwelling filament met the warm tongue, forming a sharp temperature front and a line of strong shear (SS') between the southeastward flowing filament and the northwestward flow in the eddy. The eddy center was as cold as the filament of upwelled water.

In the corresponding SAR image (Figure 7b) structure in the surface roughness field extended several island diameters south of Gran Canaria. Unfortunately, no simultaneous in situ observations could be made to confirm identification of the offshore wind shear lines. A 3-4 km wide band of winds below the 3 m s^{-1} SAR threshold was evident near the southwest coast, where midday coastal winds registered 2-3 m s^{-1} onshore. Backscatter was strong along the anticyclonic wind shear line extending southwest from near Arguineguin (TT'T"), farther west than is normally encountered. The western cyclonic shear boundary was evident as a weak contrast in the image.

In Figure 7b a series of alternating bright and dark bands, situated on the eastern side of TT'T", have diffuse edges, suggesting atmospheric structures. Their eastern limit was ill defined, while the western limit was clearer in the north, where it coincided with the edge of the warm tail TT' (Figure 7a). It continued north in a curve along the eastern bound of the warmest wake waters to intersect the shore. The spacing of the banding, 2 - 5 km, was compatible with thermally forced horizontal roll vortices formed preferentially over the warm tail and extending at a small angle downwind [LeMone, 1973]. Given the reported inversion layer height of 800 m at Tenerife, the horizontal to vertical aspect ratio would be ~ 3:1 for such structures, as observed. However, the structures seem analogous to a shallow water ship wake, with a series of transverse waves decaying away from the disturbance point apparently near point T. Although the supporting information is meager, the structures appear to originate at the height of the inversion layer.

Another elongated bright line SS' represents a localized current shear along the temperature front between the southeastward flowing filament and the northwestward moving warm tongue entrained around the eddy. Fu and Holt [1983] reported similar structure in a Seasat SAR image in relation to an offshore intrusion of upwelled water off California. A similar, if weaker, bright line F could be identified near the eastern edge of the southern cold core in the filament near 27.3°N, 15.5"W, again presumably associated with localized current shear. The cyclonic eddy centered at 27.4°N, 16.3°W produced no signal in the SAR image.

In the northwest of the image (Figure 7b) a streaked appearance indicates wind rows, indicative of the predominant wind direction [Johannessen et al., 1995]. This parallelled the wind direction at the exposed east coast stations and was consistent over a wide area, in agreement with surface pressure (Figure 2a) and scatterometer winds (Plate 1a). Wind rows were also seen in the southeast of the image but not in the lee, where wind direction is variable. Finally, a group of atmospheric gravity waves (GW) was identifiable near 27.7°N, 16.1"W. About eight waves of wavelength 2.5 km and crest length < 15 km were discernible in the group.

An estimate of wind speed is possible from the SAR backscatter intensity if a wind direction is known (or assumed) at each point in the image. An overall direction of 203" was taken on the basis of coastal winds, the wind row orientation, the scatterometer analysis, and daily meteorological charts. The structure of the wind field immediately downstream of the island is unknown, so these results do not strictly apply to the lee region. Estimating directions in small areas of the image from the orientation of wind rows [Lehner et al., 1998], which are generally aligned with the wind, was impossible since in the lee region no defined windrows were visible. The calibrated backscatter values were averaged over 50 x 50 and subsampled at 25 pixel intervals, yielding wind speed estimates at 2.5 km resolution.

Estimated wind speed on July 29 (Figure 7c) reached 20 m s^{-1} on the eastern flank of the lee, suggesting significant enhancement. The higher values separated to either side of the wave-like features TT'T", and a secondary maximum of speed occurred well downwind near 26.7°N. Minimum speeds close to 4 m s^{-1} occurred near the lee coast, with a trough of low speeds extending southwestward. Estimated speeds outside the disturbed region were ~ 14 m s^{-1}. Values were generally higher than expected but no in situ data at sea were available for comparison. Small local differences from the assumed wind direction do not affect the speed estimate greatly, and although values in the lee can be affected significantly by erroneous assumed direction, they would not be increased to values found outside.

Figure 7d shows the near-infrared AVHRR channel 2 (0.9 μm) from NOAA 9, taken 50 min before the ERS SAR image. This channel is sensitive to solar reflection and reveals a remarkable sun glint pattern that parallels exactly the pattern of waves seen in the SAR image (Figure 7b), confirming that they are caused by wind-induced variations of surface roughness.

The AVHRR image for the following day (Figure 8a) is from the pass at 0759 UT because of extensive cloud cover later in the day. Two hours after dawn, the warm lee was barely 1°C warmer than surrounding waters. The island winds were similar to the previous day, but the extended tail of warm water was not apparent. The strong temperature contrast between the cool upwelling filament and the warm water tongue entrained around the cyclonic eddy again formed an almost rectilinear feature (SS') oriented northwest-southeast. As before, surface waters off northwest Gran Canaria were cooler than off the east coast.

The SAR image for July 30 (Figure 8b) shows particularly clearly a wake-like feature that extends downwind almost 200 km. Dark areas close to the south coast of Gran Canaria indicate regions of wind below the threshold value of 3 m s^{-1} (confirmed by the adjacent coastal wind vectors). The calm zone was larger than on the previous day. The boundaries of the lee appear as linear features contrasting in brightness with
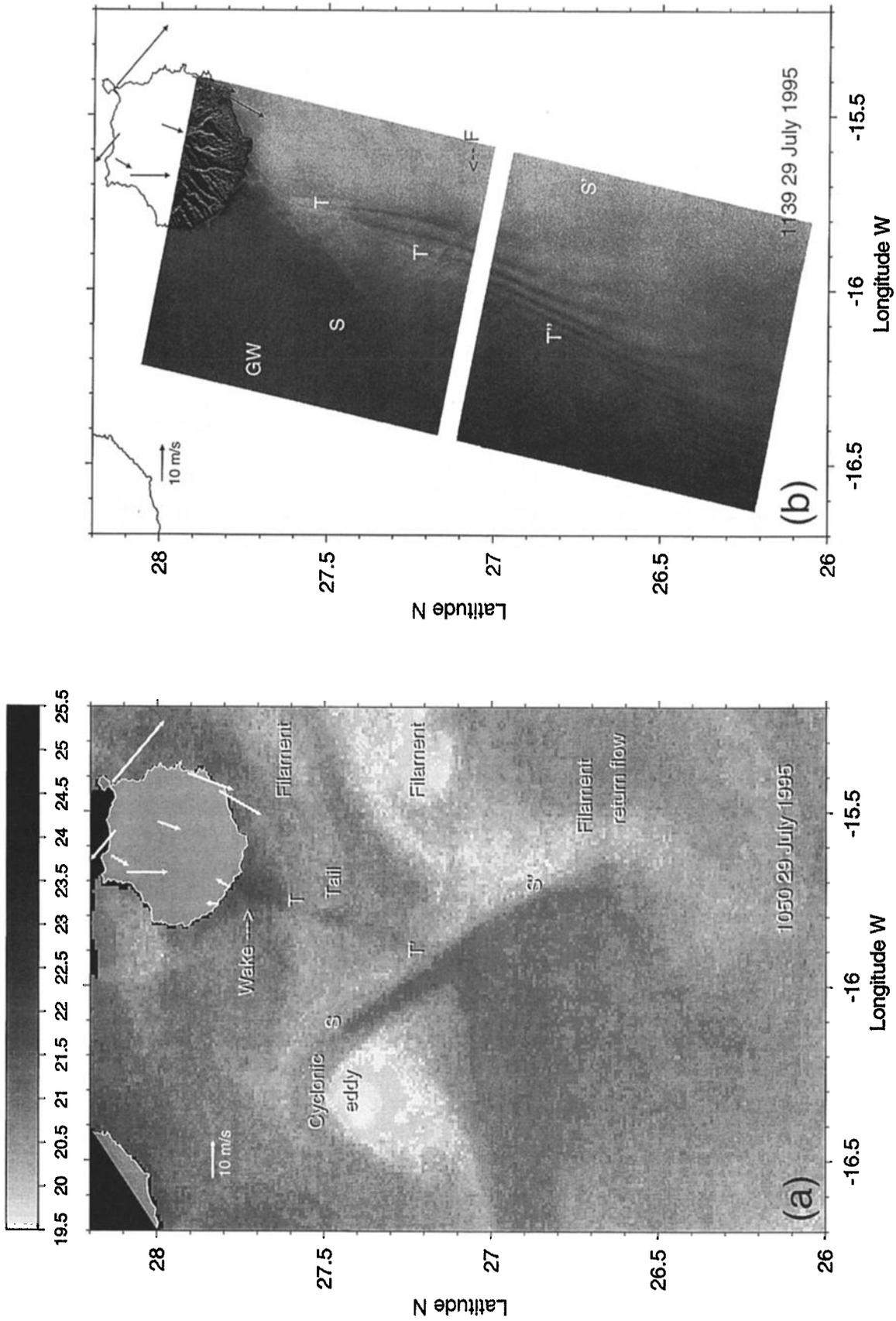
Figure 7. (a) AVHRR SST image for July 29. (b) SAR image of the same day. (c) Derived CMOD4 wind. (d) Near-infra red (channel 2) AVHRR in units of %albedo. Midday winds at shore sites are shown in Figures 7a - 7c. Labels are explained in the text.
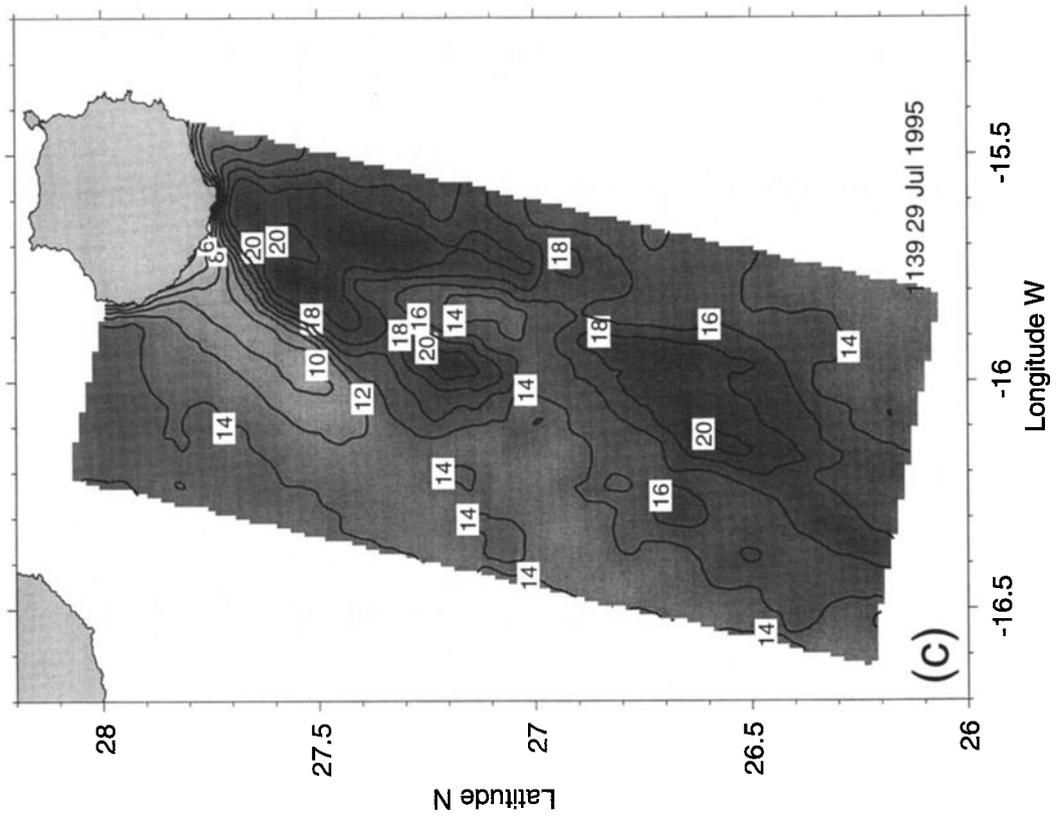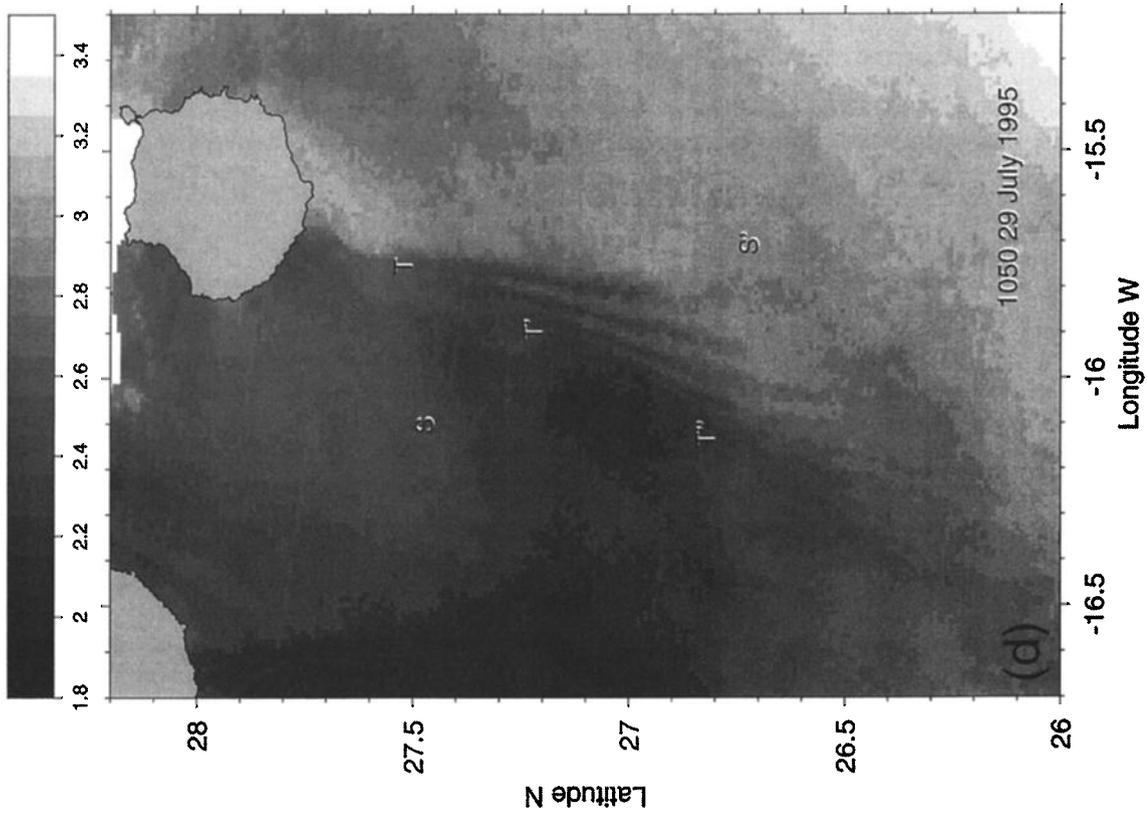
Figure 7. (continued)
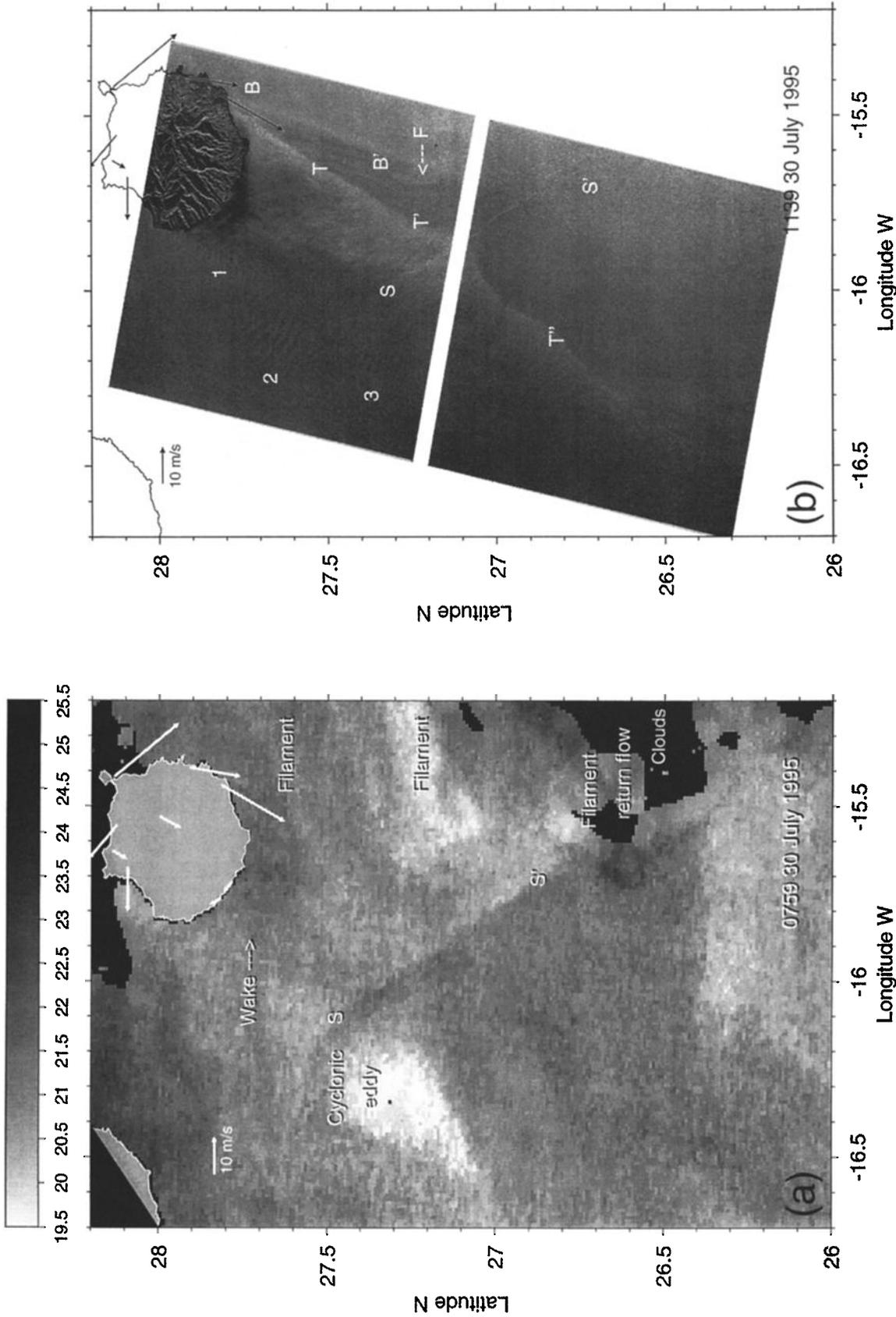
Figure 8. (a) AVHRR sea surface temperature images for July 30, (b) SAR image same day. (c) Derived CMOD4 wind. (d) In situ wind vectors for 15 days in August 1993 from R/V *Hesperides* overlaid on speed contours from same data set. The midday winds at shore sites are shown in Figures 8a - 8c. Labels are explained in the text.
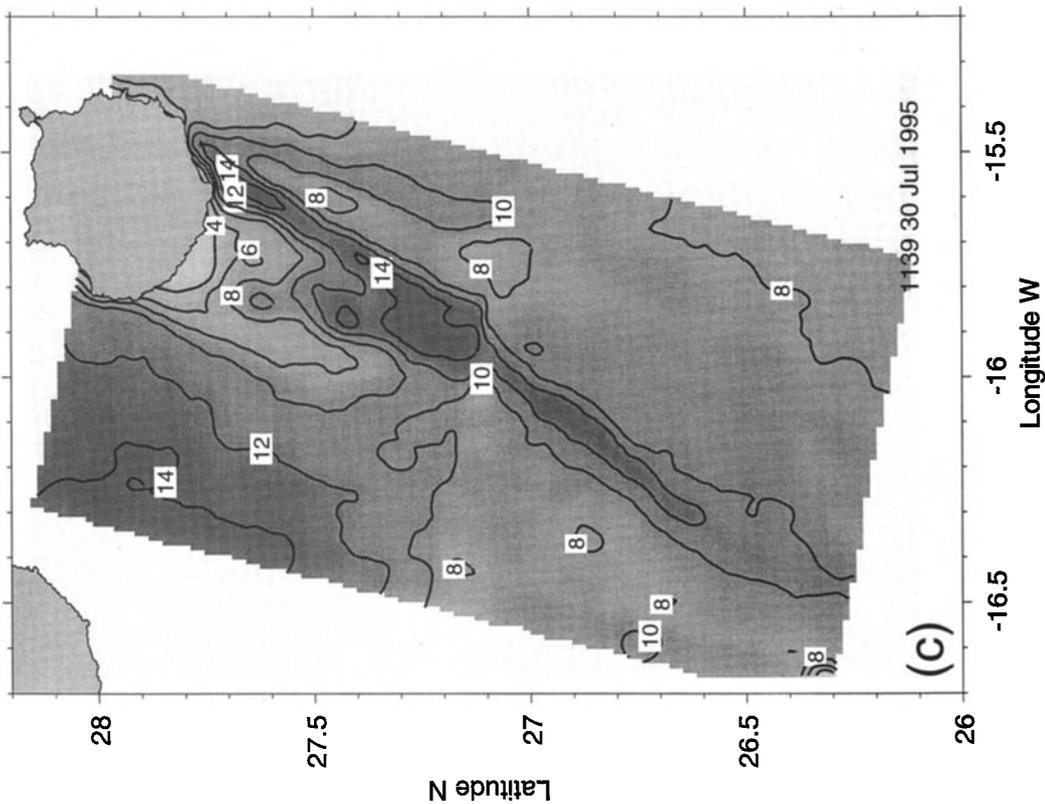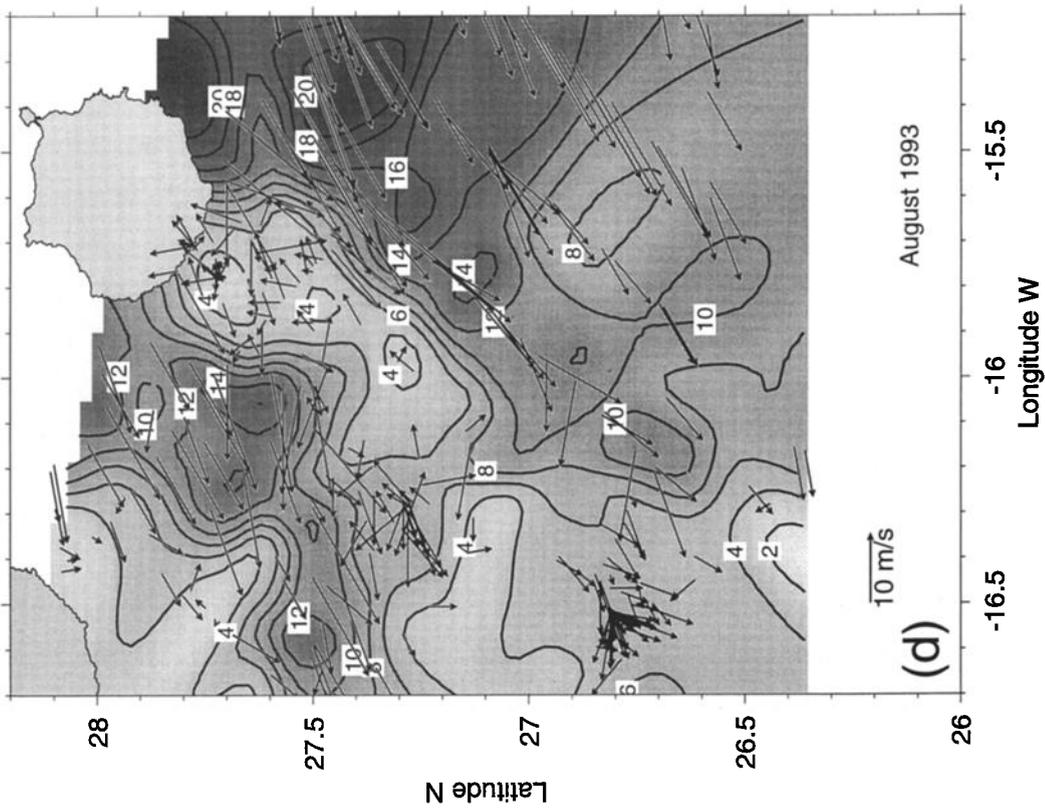
Figure 8. (continued)

surrounding areas. The eastern (anticyclonic) boundary TT'T" is especially clear as a bright streak some 2 km wide and 180 km long parallel to the wind at the southeastern coast. The boundary had shifted 15-20 km eastward near the island.

The main bright boundary corresponds to the edge of the trade wind zone. About 100 km south of the island, where it intersected the current shear line SS', the orientation of the boundary changed, possibly as a result of changing atmospheric stability above the warm tongue. A weaker bright line BB', ~80 km long, diverged from the first on the southeast coast of Gran Canaria. Between the two, six darker bands parallel to the secondary front seem to be weakened examples of the wave-like structures of the previous day. BB' is likely therefore the diffuse eastern boundary. The current shear SS' had hardly moved from the previous day. A second bright line F (shown in zoom in Figure 9a) coincided with another temperature front on the western limit of the southern filament, again indicating strong horizontal shear.

The western (cyclonic) boundary, as a location of surface Ekman divergence, was less well defined but detectable as a broad, almost rectilinear feature of weak contrast. It extended southward from Punta Descojonado through S to converge with the eastern boundary near the break between SAR frames. The western half of the image shows many wind rows at separations of 2 - 4 km aligned along the predominant wind direction (close up in Figure 9b) as in the previous day's image.

Southwest of Gran Canaria, atmospheric internal wave packets (1, 2, and 3) emanate from near Punta Descojonado toward the southwest. The series is visible as several diffuse groups of lighter and darker bands oriented northwest-southeast with a crest length that is short (about 6 km) nearshore but increases with distance from the coast. The separation between the 6 - 10 diffuse crests in each group is ~ 3 km. The most offshore group is ~ 90 km southwest of the island. Group 2 is detailed in Figure 9c.

SAR wind speed estimates for July 30 (Figure 8c) were lower than the previous day, except in the northwest of the region. (The assumed direction was again 203°.) Enhanced wind speed extended some 150 km southwest along the boundary TT'T", but the area of speeds near 20 m s^{-1} was small. Weaker enhancement occurred along the line BB'. The lee region was defined by winds < 10 m s^{-1} and immediately south west of the island, speeds < 3 m s^{-1} were indicated. There was some evidence of higher speeds in the lee center,

reflecting the return flow seen in the in situ measurements on other days. The lee boundaries formed zones of strong wind shear despite uncertainty in wind direction within the lee.

Although there were no contemporaneous observations of ocean winds, a composite wind field measured over 15 days in August 1993 on R/V *Hesperides* (Figure 8d) shows the existence of an extended lee with weak flow counter to the trade winds. Maximum speeds measured reached the 20 m s^{-1} indicated on July 29 1995, in similar locations. Wind speeds in the northwest were also similar to the present estimates, ~ 14 m s^{-1}. Evidence of sheltering by the nearby island of Tenerife was also indicated. The 1993 wind field is not nearly, synoptic and the sparse observations limit interpretation, but the strong similarities with the SAR wind fields are encouraging.

4. Discussion

Biological enhancement around oceanic islands was established by *Doty and Ogury* [1956], but its physical causes are less well known. The role of oceanic islands in producing disturbances in the downstream current has been investigated in a number of cases. *Barkley* [1972] concluded that drifter tracks downstream of Johnson's Atoll in the Pacific North Equatorial Current were consistent with a von Karman vortex street. Other observations have indicated disturbance of the equatorial undercurrent east of the Galapagos [*White*, 1973] and production of eddies west of the Hawaiian Islands [*Patzert*, 1969; *Lumpkin*, 1998; *Flament et al.*, 1998]. *Heywood et al.* [1990] found an eddy trapped behind Aldabra Atoll in the Indian Ocean South Equatorial Current. Frequent production of, principally, cyclonic eddies south of Gran Canaria has been reported by *Arístegui et al.* [1994, 1997]. Theoretical and laboratory studies [e.g. *Boyer and Davis*, 1982; *Bearman*, 1984; *Sangrá*, 1995; *Heywood et al.*, 1996] show the Earth's rotation delays eddy shedding to higher Reynolds numbers and makes the vortex street asymmetrical by enhancing cyclonic eddies in the Northern Hemisphere. For islands like Aldabra Atoll, with low topographic relief, downstream flow effects clearly result from the direct disturbance of the current field by the island. This is less obvious for mountainous islands, where strong wind regimes may be perturbed to provide a second source of disturbance to the oceanic flow [*Patzert*, 1969].

In the present case, an extended and variable region sheltered from the trade winds is present behind Gran Canaria
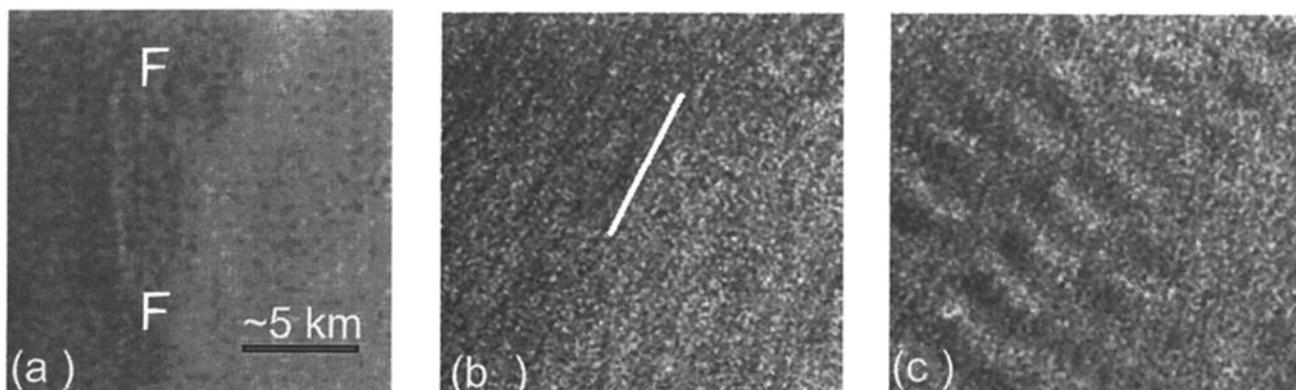
Figure 9. Enhanced close ups of SAR image of July 30 1995: (a) Shear front F, (b) wind rows in NW of image (the line is oriented at 205") and (c) group 2 of the lee waves. The approximate distance scale is shown in Figure 9a.

(and the other Canary Islands). This lee was evident in AVHRR imagery as a warm surface temperature anomaly due to the dominance of surface heating over wind mixing. The extent of the temperature gradients that bound the lee suggests that the lines of intense wind shear persisted some 100 km or more downwind. The direct observations indicated that a weak return breeze cools the center of the lee, separating two temperature maxima beneath the areas of weakest wind. This is compatible with the presence of counterrotating wind eddies behind the island.

Chopra [1973], from mesoscale patterns in stratocumulus cloud, concluded that atmospheric vortices of 10-20 km radius were shed from alternate flanks of Gran Canaria at roughly 8 hour intervals, as in a von Karman vortex street. These structures formed a wake 60 km wide and 600 km long as they drifted downwind at some 70% of the ambient wind speed. Viscous forces made individual vortices expand, weaken, and disappear after about 30 hours. The observed shift in position of the eastern lee boundary between July 29 and 30 may result from atmospheric eddy shedding, although the wind direction could not be determined from the SAR images.

Atmospheric phenomena associated with the lee region, including mountain lee waves, convective rolls, and strong shears in the atmospheric boundary layer, are revealed by the SAR images. The atmospheric internal gravity (or mountain lee) waves arise near Punta La Aldea, the westernmost part of the island, where the winds strike shear cliffs rising hundreds of meters from the sea. Cap clouds frequently form as the wind passes over the 400 m high coastal peaks before descending to cross a 5 km wide valley and rising again over the 600 m high ridges between La Aldea and Descojonado (Figure 1). No similar wave-like features are seen on the east of the island, where a wide coastal plain slopes gradually into the island interior. Internal waves in the relatively low inversion layer are associated with fluctuations in wind velocity extending down to sea level [Vachon et al., 1995]. Beneath troughs, increased wind velocity and sea surface roughness produces brighter bands in the SAR image, while under troughs, decreased velocity produces darker bands.

Zones of temperature contrast and current shear were also visible in the SAR images even though the radar intensity arises mainly from Bragg backscatter by the ~3 cm wind-driven capillary waves. When the 10 m wind is below a threshold value of ~ 3 m s^{-1}, there is no appreciable return signal [Donelan and Pierson, 1987], as observed in the nearshore lee. Gower [1994] reported that for winds between 2 and 5 m s^{-1}, surface slicks indicating patterns of current convergence may appear, but that at higher wind speeds, current-related features are obscured by the wind signal. Beal et al. [1997] identified Gulf Stream current features in SAR images when wind was < 10 m s^{-1}. In our case the shear line (SS' in Figs 7 and 8) was evident in winds up to 15 m s^{-1}, suggestive of unusually strong shear.

Current gradients across shear and convergence zones may interact with short surface gravity waves, produce refraction of long surface waves, cause wave breaking, and enhance surface roughness [Robinson, 1985]. The anticyclonic wind shear line was particularly evident in the SAR image of July 30 (Figure 8). This zone is visible at sea as a region of intense white capping and chop and a locus of convergence. The enhanced roughness may result in overestimation of the CMOD4 wind speed on the lee boundary. The air-sea temperature difference may reduce the accuracy of the speed estimates [Apel, 1994], especially in the lee where the sea surface temperature is

higher. Beal et al. [1997] found consistent backscatter differences caused by spatial variability of the marine atmospheric boundary layer stability.

Close to the island, a warm surface wake in the wind lee persisted throughout the observation period, strengthening during the day and weakening at night. Outside the lee, surface heat input is distributed through a well-mixed surface layer, while inside, near-surface stratification develops. Nighttime convective overturning distributes the day time input over the shallower layers. The CTD sections showed upwelling of the pycnocline as expected close to the cyclonic wind shear line, but the greatest pycnocline depression was displaced toward the center of the lee in one section. This may be caused by an approach of the filament closer to the island. Since density surfaces in the upwelled filament waters are shallower than in oceanic waters, the filament would tend to counteract downwelling on the anticyclonic boundary of the lee. The position of maximum deepening therefore varies with the strength and position of the filament and with the wind. Variability of the filament has been reported by Arístegui et al. [1997] who have shown significant effects on the local biology. Salinity in the island lee results from the interplay between the upwelling filament and oceanic background flow. The salinity field seems to be separated into two halves across the wake, corresponding to waters from different sources, including the filament.

What is the relative importance of Ekman pumping and flow disturbance in producing the eddies? A well-defined wind lee is evident even in the several week composite wind field, so that mean Ekman forcing must be significant despite any short term variability caused by vortex shedding. On the lee boundaries, horizontal wind shear of 15 m s^{-1} per 2 km produces upwelling (or downwelling) as strong as that seen at the African coast; upwelling occurs on the exposed western coasts of the islands. The Ekman transport caused by 10 (15) m s^{-1} wind with a drag coefficient of 1.3 x 10^{-3} at 28°N is 1.9 (4.3) m^2 s^{-1}, which would cause upwelling (or downwelling) of 11 (24) m d^{-1}, assuming a constant rate over a Rossby radius of 15 km. Because of the lack of a solid boundary downstream, this upwelling or downwelling of the pycnocline will produce eddies on a length scale of the lee.

Even intermittent wind forcing, as in the Gulf of Tehuantepec, can produce energetic ocean eddies [Barton et al., 1993; Trasviña et al., 1995]. There, winds channelled through a mountain pass extend as a jet over the Pacific Ocean and spin up ocean eddies. Since there is no significant background current in the area, the Ekman pumping is the direct cause of the eddies. Even in the presence of currents, wind forcing has been reported to spin up eddies north of Hawaii [Patzert, 1969; Lumpkin, 1998]. Chopra [1973] stressed that vertical transfer of momentum to the ocean would weaken any vortices below the atmospheric inversion too quickly to form a vortex street. He interpreted Patzert's [1969] conclusion that the Hawaiian ocean eddies were wind driven as the explanation for the absence of an atmospheric vortex street, although subsequent observations show one to be present at times.

Here the existence of a cyclonic oceanic eddy downstream and a variable lee in the wind is clearly documented. The eddy, generated close to the island, moved southwestward at 5 km d^{-1} as its surface temperature signal weakened over the course of 12 days. Mutually exclusive ocean eddies and atmospheric vortices could, of course, exist at different times.

Wind downstream of Gran Canaria is persistent and strong so may be expected to produce or at least enhance oceanic eddies.

This area of filament-eddy exchanges provides an excellent laboratory: the repeatability and steadiness of the trade wind regime provides continuous forcing of coastal upwelling and filaments, while eddies reportedly spin off from Gran Canaria during most of the year. Both cyclonic and anticyclonic eddies have been observed south of the island; indeed, recent drifter observations have followed an anticyclone for 7 months as it drifted away from the island (P.Sangrá, *personal communication*, 1999). Interaction between eddies, filaments, and the island chain give rise to strong horizontal gradients and to lateral exchange of properties within a small geographical area. These can be of considerable significance for distribution of, say, larval distributions [*Rodríguez et al.*, 1999] or zooplankton [*Hernández-León*, 1988]. However, there have been no observations of eddy generation: details of their development, eventual fate, and how they interact with filaments remain poorly known.

References

Apel, J., An improved model of the ocean surface wave vector spectrum and its effects on radar backscatter, *J. Geophys. Res.*, 99, 16,269-16,291, 1994.

Arístegui, J., P. Sangrá, S. Hernández-Leon, M. Cantón, A. Hernández-Guerra and J.L. Kerling, Island-induced eddies in the Canary Islands, *Deep Sea Res., Part I, 41*, 1509-1525, 1994.

Arístegui, J., et al., The influence of island-generated eddies on chlorophyll distribution: A study of mesoscale variation around Gran Canaria, *Deep Sea Res., Part I, 44*, 71-96, 1997.

Barkley, R.A., Johnston Atoll's wake, *J. Mar. Res., 30*, 201-216, 1972.

Barton, E.D., M.L. Argote, J. Brown, P.M. Kosro, M. Lavín, J.M. Robles, R.L. Smith, A. Trasviña, and H.S. Vélez, Supersquirt: Dynamics of the Gulf of Tehuantepec, Mexico, *Oceanography, 6*, 23-30, 1993.

Barton E.D., et al., The transition zone of the Canary Current upwelling region, *Prog. Oceanogr., 41*, 455-504, 1998.

Beal, R.C., V.N. Kudryavtsev, D.R. Thompson, S.A. Grodsky, D.G. Tilley, V.A. Dulov, and H.C. Graber, The influence of the marine atmospheric boundary layer on ERS-1 synthetic aperture radar imagery of the Gulf Stream, *J. Geophys. Res., 102*, 5799-5814, 1997.

Bearman, P.W., Vortex shedding from oscillating bluff bodies, *Ann. Rev. Fluid Mech., 16*, 195-222, 1984.

Boyer, D.L., and P.A. Davis, Flow past a circular cylinder on a β-plane, *Philos. Trans. R. Soc., London, Ser. A, 322*, 213-241, 1982.

Chopra K.P., Atmospheric and oceanic flow problems introduced by islands, *Adv. Geophys., 16*, 297-421, 1973.

Columbus, C., *The Log of Christopher Columbus*, translated from the Spanish by R.H. Fuson, 252 pp,. Ashford, Southampton, England, U.K., 1987.

Donelan, M.A., and W.J. Pierson Jr., Radar scattering and equilibrium ranges in wind generated waves with application to scatterometry, *J. Geophys. Res., 92*, 4971-5029, 1987.

Doty, M.S., and M. Oguri, The island mass effect, *J. Cons. Perm. Int. Explor. Mer., 22*, 33-37, 1956.

Flament, P., J. Firing, M. Sawyer, and C. Trefois, Amplitude and horizontal structure of a large diurnal sea surface warming event during the coastal ocean dynamics experiment, *J. Phys. Oceanogr., 24*, 124-139, 1994.

Flament, P., S.C. Kennan. C.Lumpkin, and E.D. Stroup, The Atlas of Hawai'i, in *The Ocean*, edited by S. Juvik and J. Juvik, pp. 82-86, University of Hawai'i Press, Honolulu, 1998.

Fleming, H.E., and M.L. Hill, An objective procedure for detecting and correcting errors in geophysical data, 1., One-Dimensional applications, *J. Geophys. Res., 87*, 7312-7324, 1982.

Fu, L.-L., and B. Holt, Some examples of detection of oceanic mesoscale eddies by the Seasat Synthetic Aperture Radar, *J. Geophys. Res., 88*, 1844-1852, 1983.

Gower, J.F.R., Mapping coastal currents with SAR using naturally occurring surface slick patterns, Eur. Space Agency Spec. Publ., *ESA SP-361*, 415-418, 1994.

Hernández-Guerra, A., Estructuras oceanográficas observadas en las aguas que rodean las Islas Canarias mediante escenas de los sensores AVHRR y CZCS. Ph.D. thesis, 198 pp., Univ. de Las Palmas de Gran Canaria, Las Palmas de Gran Canaria, Spain, 1990.

Hernández-Guerra, A., J. Arístegui, M. Cantón, and L. Nykjaer, Phytoplankton pigment patterns in the Canary Islands as determined using Coastal Zone Color Scanner data, *Int. J. Remote Sens., 14*, 1431-1437, 1993.

Hernández-León, S., Gradients of mesozooplankton biomass and ETS activity in the wind-shear area as evidence of an island mass effect in the Canary Island waters, *J. Plankton Res., 10*, 1141-1154, 1988.

Heywood, K.J., E.D. Barton ,and J.H. Simpson, The effects of flow d isturbance by an oceanic island, *J. Mar. Res., 18*, 55-73, 1990.

Heywood, K.J., D.P. Stevens, and G.R Bigg, Eddy formation behind the tropical island of Aldabra , *Deep-Sea Res., Part I, 43*, 555-578,1996.

Johannessen, J.A., R.A. Shuchman, and O.M. Johannessen, Synthetic aperture radar on ERS-1, in *Oceanographic Applications of Remote Sensing*, edited by M. Ikeda and F.W. Dobson, pp. 27-44, CRC Press, Boca Raton, Fla., 1995.

Koch, S.E., M. DesJardins, and P.J. Kocin, An interactive Barnes objective map analysis scheme for use with satellite and conventional data, *J. Clim Appl. Meteorol., 22*, 1487-1503, 1983.

Laur, H., P. Bally, P Meadows, J. Sanchez, B. Schaettler, and E. Lopinto, Deviation of the Backscattering Coefficient σ_0 in ESA ERS PRI products, *ESA Doc. ES-TN-RS-PM-HL09, Vol. 2*, 4, pp.87, Eur. Space Agency, Paris, 1997.

Lehner, S., J. Horstmann, W. Koch, and W. Rosenthal, Mesoscale wind measurements using recalibrated ERS SAR images, *J. Geophys. Res., 103*, 7847-7856, 1998.

LeMone, M.A., The structure and dynamics of horizontal roll vortices in the planetary boundary layer, *J. Atmos. Sci., 30*, 1077-1091, 1973.

Lentz, S.J., The surface boundary layer in coastal upwelling regions. *J. Phys. Oceanogr., 22*, 1517-1539, 1992.

Le Traon, P. Y., P. Gaspar, F. Bouyssel, and H. Makhmara, Using

TOPEX/Poseidon data to enhance ERS-1 data, *J. Atmos. Oceanic Technol., 12*, 161-170, 1995.

Lumpkin, C.F., Eddies and currents of the Hawaiian Islands, Ph.D. thesis, 281 pp., Univ. of Hawaii at Manoa, Honolulu, 1998.

McClain, E.P., W. Pichel, and C. Walton, Comparative performance of AVHRR-based multichannel sea surface temperatures, *J. Geophys. Res., 90*, 11,587-11,601, 1985.

Meadows, P., and P.A. Wright, ERS-1 SAR analogue to digital converter saturation, Paper presented at CEOS SAR Calibration Workshop Comm. On Earth Obs. Sat., Ann Arbor, Michigan, Sept. 28-30,1994.

Molina, R., and F.L. Laatzen, Hidrografía en la región Canaria: Campaña Canarias I, *Bol. Inst. Esp. Oceanogr., 5*, 71-86, 1989.

Molina, R., J.M. Cabanas, and F.L. Laatzen, Corrientes e hidrografía en la región Canaria: Campaña Canaria 9205, *Bol. Inst. Esp. Oceanogr.,* 121, 43-52, 1998.

Navarro-Pérez, E., Physical oceanography of the Canary current: Short term, seasonal and interannual variability, Ph D. thesis, Univ. of Wales, Bangor, 1996.

Navarro-Pérez, E., and E.D. Barton, The physical structure of an upwelling filament off the north-west African coast during August 1993, *S. Afr. J. Mar. Sci., 19*, 61-74, 1998.

Naya, A., *Meteorología Superior*, 546 pp., Espasa-Calpe, Madrid, 1984.

Patzert, W.C., Eddies in Hawaiian waters, *Rep. HIG-69-8*, 51 pp., Hawaii Inst. of Geophys., University of Hawaii at Manoa, Honolulu, 1969.

Pollard, R., P.B. Rhines, and R.O.R.Y. Thompson, The deepening of the wind-mixed layer, *Geophys. Fluid Dyn., 3*, 381-404, 1973.

Robinson, I.S., *Satellite Oceanography: An Introduction for Oceanographers and Remote-Sensing Scientists*, 455 pp., Ellis-Horwood, New York, 1985.

Rodríguez, J.M., S. Hernández-León, and E.D Barton, Mesoscale distribution of fish larvae in relation to an upwelling filament off northwest Africa, *Deep Sea Res., Part I*, 46, 1969-1984, 1999.

Sangrá, P., Pertubación de un flujo geofísico por un obstáculo: aplicación a la isla de Gran Canaria, Ph.D. thesis, 200 pp., Univ. of Las Palmas de Gran Canaria, Las Palmas de Gran Canaria, Spain, 1995.

Saunders, R.W., and K.T. Kriebel, An improved method for detecting clear sky and cloudy radiances from AVHRR data, *Int. J. Remote Sensing*, 9, 123-150, 1988.

Stoffelen, A.D., and D.L.T. Anderson, Scatterometer data interpretation: Estimation and validation of the transfer function CMOD4, *J Geophys. Res., 102*, 5767-5780, 1997.

Trasviña, A., E.D Barton., J. Brown, H.S. Velez, P.M. Kosro, and R.L. Smith, Offshore wind forcing in the Gulf of Tehuantepec, Mexico: the asymmetric circulation, *J. Geophys. Res., 100*, 20,649-20,663, 1995.

Vachon, P.W., J.A. Johannessen and D.P Browne, ERS-1 SAR Images of atmospheric gravity waves, *IEEE Trans. Geosci. Remote Sens., 33*, 1014-1025, 1995.

Van Camp, L., L. Nykjaer, E. Mittelstaedt, and P. Schlittenhardt, Upwelling and boundary circulation off northwest Africa as depicted by infrared and visible satellite observations, *Prog. Oceanogr., 26*, 357-402, 1991.

White, W.B., An oceanic wake in the undercurrent downstream from the Galapagos Archipelago, *J. Phys. Oceanogr., 3*, 156-161, 1973. 1992.

J.Aristegui and G. Basterretxea, Facultad de Ciencias del Mar, Universidad de Las Palmas de Gran Canaria, 35017, Las Palmas de Gran Canaria, Spain. (javier.aristegui@biologia.ulpgc.es; gotzon.basterretxea@songoku.uib.es)

E.D. Barton (corresponding author), School of Ocean Sciences, University of Wales, Bangor LL59 5 EY, Wales, U.K. (e.d.barton@sos. bangor.ac.uk)

P. Flament, Department of Oceanography, University of Hawaii at Manoa, Honolulu, HI 96822. (pierre@hawaii.edu)

F. Herrera, Laboratorio de Comunicaciones y TeledetecciOn, Universidad de La Laguna, Tenerife, Spain. (fherrera@ull.es terascan@ull.es)

B. Jones and E. G. Mitchelson-Jacob, Unit for Coastal and Estuarine Studies, University of Wales, Bangor LL59 5EY, Wales, U.K. (b.jones@bangor.ac.uk;e.g.mitchelson-jacob@bangor.ac.uk)